Quasi-Biweekly Mode and Its Modulation on the Diurnal Rainfall in Taiwan Forecasted by the CFS

SHIH-YU WANG

Utah Climate Center, and Department of Plants, Soils, and Climate, Utah State University, Logan, Utah

HSIN-HSING CHIA*

Central Weather Bureau, Taipei, Taiwan

ROBERT R. GILLIES

Utah Climate Center, and Department of Plants, Soils, and Climate, Utah State University, Logan, Utah

XIANAN JIANG

*Joint Institute for Regional Earth System Science and Engineering, University of California,
Los Angeles, Los Angeles, California*

ABSTRACT

The occurrence of diurnal afternoon convection in Taiwan undergoes substantial modulation from tropical intraseasonal oscillations in the western North Pacific, including the quasi-biweekly (QBW) mode. By analyzing surface station observations and the Climate Forecast System (CFS) Reanalyses (CFSR), as well as the NCEP CFS version 2 (CFSv2) reforecast data over 18 summers from 1993 to 2010, it was found that the QBW mode plays a significant role in the formation of episodic diurnal convection. When the cyclonic circulation of the QBW mode is located west of Taiwan, followed by an anticyclonic circulation to the east, Taiwan's diurnal convection activity tends to intensify and persists for about 4–7 days. Synoptically, this situation reflects the enhanced subtropical anticyclone leading to fair weather conditions and increased monsoon southwesterly winds moistening the lower troposphere, all of which are conducive to thermally induced diurnal convection in Taiwan. The opposite situation tends to suppress the diurnal convection activity for a sustained period of time. Based upon this synoptic linkage, an empirical relationship between the precipitation diurnal amplitude and low-level circulation fields of the CFSv2 is derived. It was found that the CFSv2 forecast exhibits an effective lead time ranging from 16 to 24 days for the QBW mode and, subsequently, diurnal convection episodes in Taiwan.

1. Introduction

Because of its location between East Asia and the western North Pacific (Fig. 1a), Taiwan experiences a complicated warm-season weather regime that consists of midlatitude frontal systems, late-spring (mei-yu) convective rainstorms, tropical cyclones, and—when all of these diminish—pronounced diurnal convection in the late afternoon (Fig. 1b) that is induced by thermal instability due to solar heating (Li et al. 1997; Yeh and Chen 1998; Johnson and Ciesielski 2002). To monitor the rainfall associated with these weather systems, Taiwan operates a fine-resolution observational network covering approximately 450 rain gauges (Fig. 1c). Through the analysis of the rain gauge data for a 13-yr period from 1993 to 2005, Wang and Chen (2008, hereafter WC08) estimated that the diurnal/afternoon convection was a significant contributor to Taiwan's precipitation (i.e., ~31%) during the May–September season, resulting, in fact, in marginally more than is produced by typhoons (28%) and mei-yu rainstorms (25%).

---

* Current affiliation: WeatherRisk Explore Inc., Taipei, Taiwan.

Corresponding author address: Shih-Yu Wang, Utah Climate Center, Utah State University, 4825 Old Main Hill, Logan, UT 84322.
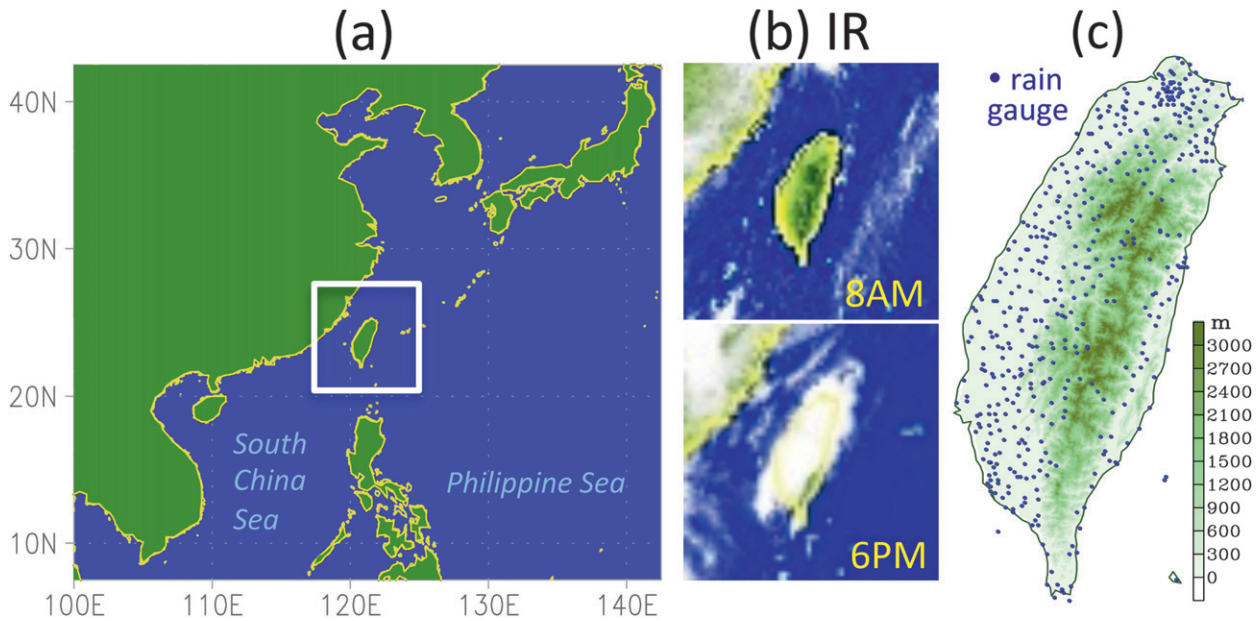E-mail: simon.wang@usu.edu

FIG. 1. (a) Map of East Asia and the western North Pacific centered over Taiwan (outlined). (b) Snapshot of infrared cloud images from a typical day during a summer diurnal convection event in the (top) morning and (bottom) evening. (c) Rain gauge network in Taiwan overlaid with terrain as shadings.

Past studies have found that the maximum hourly rainfall of diurnal convection occurs at about 1600–1700 local time (LT) along the western slopes of the mountains (e.g., Chen et al. 1999; WC08; Lin et al. 2011). In point of fact, afternoon thunderstorms in Taiwan frequently caused flash floods, traffic interruptions, and power shortages due to lightning strikes; these associated hazards have caused human casualties. However, forecasting the seemingly regular diurnal convection is challenging and it is nearly impossible to pinpoint the timing, intensity, and position of localized convective storms (Lin et al. 2012).

Taiwan's warm-seasonal rainfall features an active–break–revived life cycle that corresponds to the similar life cycle of the East Asian summer monsoon (EASM; Matsumoto 1989; Wang and LinHo 2002; Chen et al. 2004a; Ding and Chan 2005; Hsu 2005). Moreover, pronounced intraseasonal oscillations (ISOs) of convective and circulation anomalies, which vary on a time scale of 10–90 days, facilitate the formation of the monsoonal life cycle (e.g., Chen et al. 2004a). Considering the most common ISO patterns, the 30–60-day mode features a poleward propagation from the deep tropics (e.g., Lau and Chan 1986; Jiang et al. 2004), while the 10–20-day mode propagates northwestward in the western North Pacific (e.g., Nitta 1987; Fukutomi and Yasunari 1999); these two modes affect the EASM precipitation individually as well as collectively (Chen et al. 2000). Influences of these various ISO modes on

the EASM have been comprehensively studied, as has been reviewed by Chang (2004) and Lau and Waliser (2005).

In contrast, little attention has been directed toward the ISO modulation on diurnal convection. Recent work by Ichikawa and Yasunari (2006, 2008) has focused on the Maritime Continent (Borneo and New Guinea) in the deep tropics, in which diurnal convection becomes active (inactive) under lower-tropospheric westerlies (easterlies) that are controlled by the passage of the MJO. Huang and Chan (2011) showed that the diurnal and semidiurnal rainfall phases in southern China change considerably season by season. WC08 indicated that diurnal convection produces the most rainfall during the monsoon break, a synoptically inactive phase of the EASM. These aforementioned studies suggest that the properties of diurnal convection fluctuate at a variety of time scales within the EASM, possibly under the modulation of one or more ISO modes.

For many years now, the Central Weather Bureau (CWB) of Taiwan has produced an empirical forecast of the island's diurnal/afternoon thunderstorms, based upon an observed tendency that the occurrence of diurnal convection often persists for 3 days (once initiated); after that, the activity of diurnal convection tends to die out and subsequently is replaced by a prolonged period of inactivity. Focusing on northern Taiwan's diurnal convection forecast, Lin et al. (2012) also pointed out that the "persistence of yesterday's (diurnal) convective storm

activity contributed to improving today's forecast.'' The implication from these observations is that the afternoon convective activity in Taiwan may be influenced by the ISO as well.

In this paper, we investigate such an ISO influence and the feasibility of adopting a climate prediction approach to forecasting the diurnal convection episodes at the ISO time scale with a lead time of several weeks. That said, achieving credible ISO simulations with general circulation models (GCMs) still remains a challenge (e.g., Slingo et al. 1996; Waliser et al. 2003; Lin et al. 2006; Kim et al. 2009). Of late, useful predictive skill of the ISO had generally been limited to only 1–2 weeks (Hendon et al. 2000; Vitart 2009; Agudelo et al. 2006). However, in recent years, improvements in model physics, spatial resolution, and data assimilation systems have led to significant improvements in the prediction of ISO modes (Waliser 2012). For example, the National Centers for Environmental Prediction (NCEP) Coupled Forecast System (CFS) exhibits useful ISO predictive skill out to 2–4 weeks over the global domain (Zhang and Van den Dool 2012; Weaver et al. 2011). However, the CFS's forecast skill of ISO modes in the vicinity of Taiwan, particularly that associated with the 10–20-day mode during the summer, has not been extensively exploited.

In our examination of the ISO for convective occurrences in Taiwan, we first utilized an array of observational and reanalysis data to diagnose the linkage between the ISO and diurnal convection and, second, we analyzed reforecast data from the NCEP CFS model to evaluate the forecasts of the episodic feature associated with diurnal convection; these datasets are introduced in section 2. The diagnostic analyses are presented in section 3. The forecast evaluation is discussed in section 4. A summary and some conclusions are provided in section 5.

2. Data sources

The majority of the observational network in Fig. 1c belongs to the Automatic Rainfall and Meteorological Telemetry System (ARMTS), which consists of ~350 rain gauges and has been operational since 1993. The rest of the network is composed of CWB weather stations, along with agricultural, forestry, defense, hydrological, environmental, and aviation monitoring stations (WC08). For meteorological variables including winds, pressure, humidity, and temperature, we used the NCEP Climate Forecast System Reanalysis (CFSR; Saha et al. 2010) that outputs 6-hourly variables at 1.0° resolution. The analysis period spans 1993–2010. For climate prediction evaluation, we utilized the NCEP Climate Forecast System version 2 (CFSv2), which is an update of
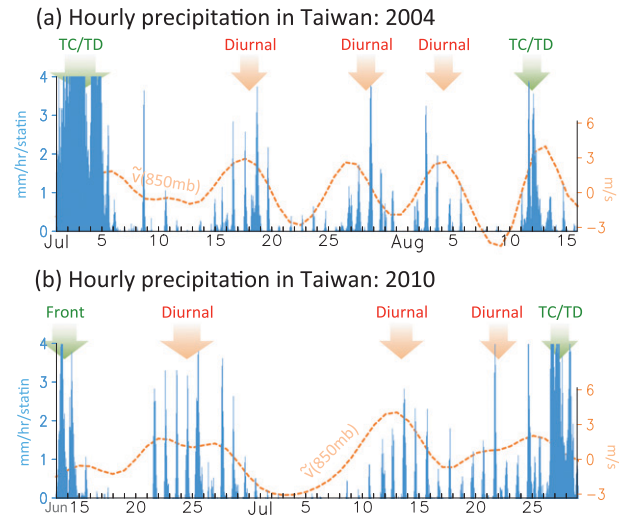

FIG. 2. (a) Hourly precipitation (cyan histogram) averaged over Taiwan during 1 Jul–15 Aug 2004, overlaid with the bandpass-filtered v wind at 850mb ($\tilde{v}$: orange dashed line). (b) As in (a), but for 15 Jun–31 Jul 2010. The diurnal convection episodes and synoptic weather events are indicated by arrows at top of panel. Diurnal convection is perceived from the sharp spikes in the precipitation histogram. Passages of tropical cyclones/depressions are denoted as TC/TD; frontal passages are indicated by ''Front.''

the earlier version (Saha et al. 2006). The CFSv2 produces a set of retrospective forecast data (or a reforecast) with a 6-hourly interval each day beginning in 1999. Other data sources included surface weather maps and infrared cloud images from the Geostationary Meteorological Satellite/Multifunctional Transport Satellites (GMS/MTSAT) series; these results were obtained from the operational outputs of the CWB (http://www.cwb.gov.tw).

3. The ISO connection with diurnal convection

a. The quasi-biweekly signal

As an example of the diurnal convection evolution, Fig. 2a shows the hourly precipitation averaged over Taiwan for the period of 1 July–15 August 2004. Two tropical cyclones passed through Taiwan during this period: one was Supertyphoon Mindulle in early July and the other was Typhoon Rananim in mid-August. In between these two typhoons, diurnal/afternoon convection events are readily discernible from the sharp ''spikes'' of hourly precipitation reflecting the afternoon maximum rainfall. Hereafter, the term *diurnal convection* refers to the afternoon maximum of precipitation. A striking feature emerges from these diurnal convection events, in the sense that they cluster into 5-day episodes such as those during 15–20 and 25–30 July, and 1–6 August. Each episode lasts about 9–11 days and

there is a clear growth–decay phase associated with all episodes, as revealed by the rising–falling peaks of diurnal rainfall. A further example is shown in Fig. 2b; this time for the summer of 2010. Likewise, the episodic feature of diurnal convection is evident (21–30 June, and 10–17 and 18–24 July), but the episodes lasted 2–4 days, longer than those of 2004. Note that the rainy spell prior to 15 June was the result of a frontal passage, while the large rainfall amount after 26 July was caused by a tropical depression (see section 3b for synoptic weather classification). These two years were selected to represent the two extreme cases in the quasi-biweekly periodicities [i.e., higher- (lower-) frequency dominated in 2004 (2010)]. In other years (not shown), such high–low frequencies were mixed in the realization of the quasi-biweekly signal.

To examine the synoptic conditions associated with the episodic behavior of Taiwan's diurnal convection, we overlaid the 850-mb daily mean meridional wind (v wind) on top of the hourly precipitation. The v wind was first averaged over Taiwan (21°–25°N, 120°–122°E) and was then bandpass filtered using the Butterworth filter with 8–25 days (Hsu and Weng 2001), in order to portray the observed low-frequency variation of diurnal convection. We used the v component of the wind (v wind) because the distribution of diurnal rainfall in Taiwan is primarily influenced by the monsoon southwesterly flow, which contributes to the concentration of precipitation along the western slope of the mountains (Yeh and Chen 1998; WC08). As is shown in Fig. 2, there is a marked correspondence between the southerly wind and active diurnal convection, and between the northerly wind and inactive diurnal convection. The predominant frequency of the v wind also coincided well with the variation frequency revealed from the diurnal convection episodes. Hereafter, this predominant time scale of 8–25 days is defined as the quasi-biweekly (QBW) mode.

The QBW time scale is further verified in Fig. 3a, which shows the power spectrum of the daily 850-mb v wind of each summer (June–August) from 1993 to 2010. While each year's power spectrum (gray lines) is different from another year, the average spectrum (black line) reveals 12–24- and 8–9-day peaks, both of which are significant at the 95% level. Another significant but weaker peak appears around 40 days and this may reflect the influence of the 30–60-day mode on the summer monsoon in Taiwan (Chen et al. 2004a). Next, based on the QBW spectral peak revealed in Fig. 3a, we bandpass filtered the surface pressure and the 850-mb streamfunction with 8–25 days and then correlated these fields with the filtered v-wind index averaged over Taiwan. Here, the filtering was performed
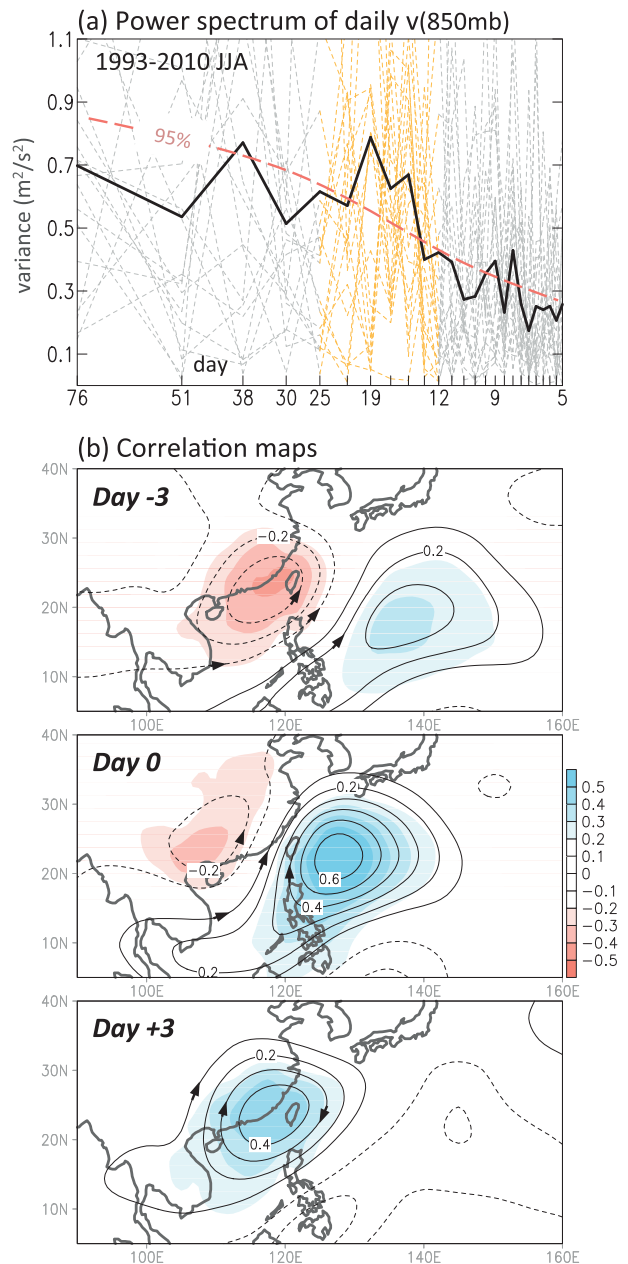

FIG. 3. (a) Power spectra of daily v wind over the summers of 1993–2010 (gray dashed lines) and their mean spectrum (solid black line). The 95% significance level averaged from all years is indicated by the pink dashed line. An individual year's spectrum within the biweekly frequency is colored in yellow. (b) Correlation maps of the bandpass-filtered 850-mb streamfunction (contours) and surface pressure (shadings) anomalies with the bandpass-filtered v-wind index. Shaded values are significant at the 95% level.

for the May–September period but May and September were excluded to avoid problems at the edges of the time series. Correlation maps (using Pearson's correlation) of surface pressure and streamfunction were computed for each year and the resulting correlation maps were

averaged over the 1993–2010 period to produce a single composite map for three time lags from day −3 to day +3.

As is evident from Fig. 3b, a circulation dipole is present at day 0 and propagates westward across Taiwan. Predominant southerly anomalous flows are inferred from the circulation dipole at day 0; this circulation dipole resembles the wave train pattern associated with the QBW mode that propagates northwestward in the Philippine Sea to near 20°N and then turns westward (e.g., Nitta 1987; Fukutomi and Yasunari 1999). Wang and Xie (1997) have suggested that the dynamics of the QBW mode involves a moist Rossby wave sustained through instability due to the easterly vertical shear, though their focus at the time was on the 20–70-day time scale. Their theory was later refined by Straub and Kiladis (2003) to include the mixed Rossby–gravity (MRG) wave that propagates northwestward. It has also been noted that a marked ocean–atmosphere interaction in these waves leads to enhanced evaporation, low-level convergence, and convection; these take place in the eastern boundary of the monsoon gyre and the life cycle of the monsoon gyre has a predominant frequency of 10–20 days (Chen et al. 2004b). These circulation features are depicted in Fig. 3b along with their association of the QBW mode from day −3 through day 0 to day +3, when the eastern portion of the cyclonic cell covers Taiwan and is presumed to prompt local convective activity.

b. Diurnal modulation of the QBW mode

The modulation of the QBW mode on the diurnal convection activity was examined through a composite analysis. The evolution of a given QBW mode can be represented equally by six phases that span the life cycle of any given QBW mode, as is illustrated in Fig. 4a. Using the QBW filtered v wind at 850 mb, six composites were made, with each phase comprising 3 days centered on the second day (note that: the spacing between each phase might vary depending on the duration of each individual QBW mode). To minimize the influence of synoptic weather events, dates with the presence of active weather in Taiwan were excluded from the composite analysis. The exclusion procedure followed that developed in WC08 and is summarized as follows:
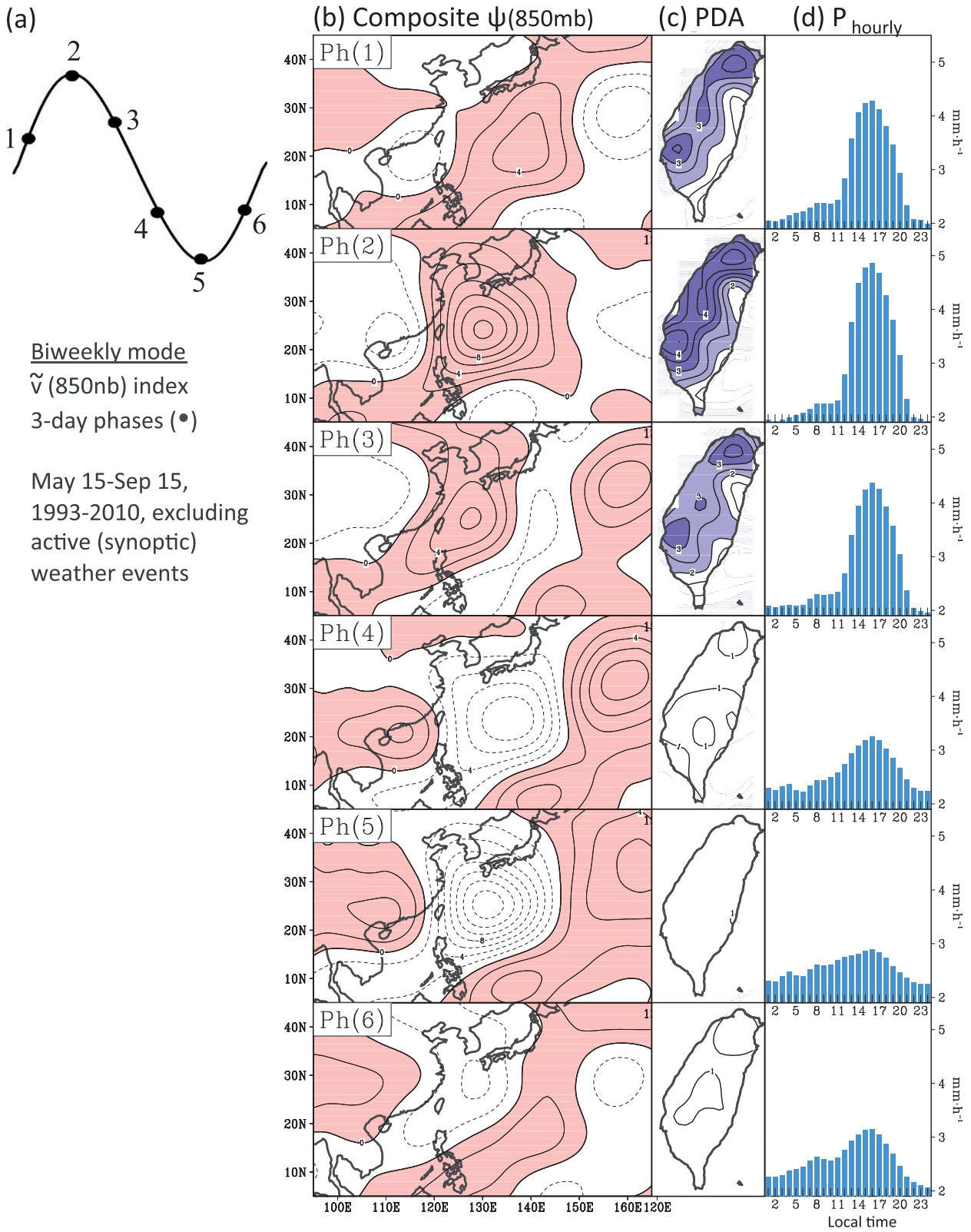
- *Frontal passage*—A cold front or stationary front is identified when the front migrates to within 50 km of Taiwan (examined from surface weather maps) and its frontal cloud band reaches the island. A complete frontal event ends when the frontal cloud band clears Taiwan.
- *Tropical cyclone/depression*—A tropical cyclone event is identified when 1) Taiwan is at least partially embedded

within the radius of 30-kt sustained wind speeds of a tropical cyclone (identified from examination of surface weather maps) or 2) tropical cyclone cloud bands covered any part of Taiwan (as viewed from IR images). A tropical depression with weaker sustained winds (<30 kt, where 1 kt $= 0.514$ m s^{-1}) was also included in this category and was identified either by use of surface weather maps or through the identification of organized convection when observed from infrared cloud images.
- *Mei-yu rainstorms*—During the mei-yu season, intense convective storms may be induced ahead of a frontal cloud band (or "prefrontal"); there, these storms develop from the interaction between southwesterly monsoon flows and migrating frontal systems (Lau et al. 2000; Lin and Kueh 2003; Wang and Huang 2009). Such storms were identified when 1) the cloud shield with a domain larger than 250 km $\times$ 250 km covered Taiwan and 2) the local rainfall rate reached 50 mm within a 6-h period at any station at any time over a 24-h period.

After removing the dates of active weather events as were identified earlier (i.e., a total of 198 days during 1995–2010), the six-phase composite of the bandpass-filtered streamfunction was compiled and is shown in Fig. 4b. During the maximum (phase 2) and minimum (phase 5) phases, the circulation dipole juxtaposing Taiwan is similar to that in Fig. 3b and the dipole appears to be embedded in a westward-propagating wave train. Next, we constructed the corresponding phase composites of the diurnal convection activity through the precipitation diurnal amplitude (PDA); this is determined by computing the difference between the maximum rainfall in the afternoon/evening hours (1300–2400 LT) and the minimum rainfall in the morning hours (0100–1200 LT) at each station. The composite PDA at each of the QBW phases was then interpolated using the Cressman scheme (Cressman 1959) with a 5-km radius of influence. As is shown in Fig. 4c, the maximum PDA occurs at phase 2 and is mainly distributed over western Taiwan along the mountain slopes; this is consistent with the diurnal rainfall distribution shown in WC08. The minimum PDA takes place at phase 5. Correspondingly, the evolution of hourly precipitation over Taiwan (Fig. 4d) reveals a significant contrast in the afternoon exists between phases 2 and 5. Since all active weather has been excluded from these composites, the results in Fig. 4 are evidence of a strong association between the PDA fluctuation and the QBW mode.

The tropospheric conditions associated with the QBW mode evolution across Taiwan were examined and are plotted in Fig. 5 as vertical cross sections of relative
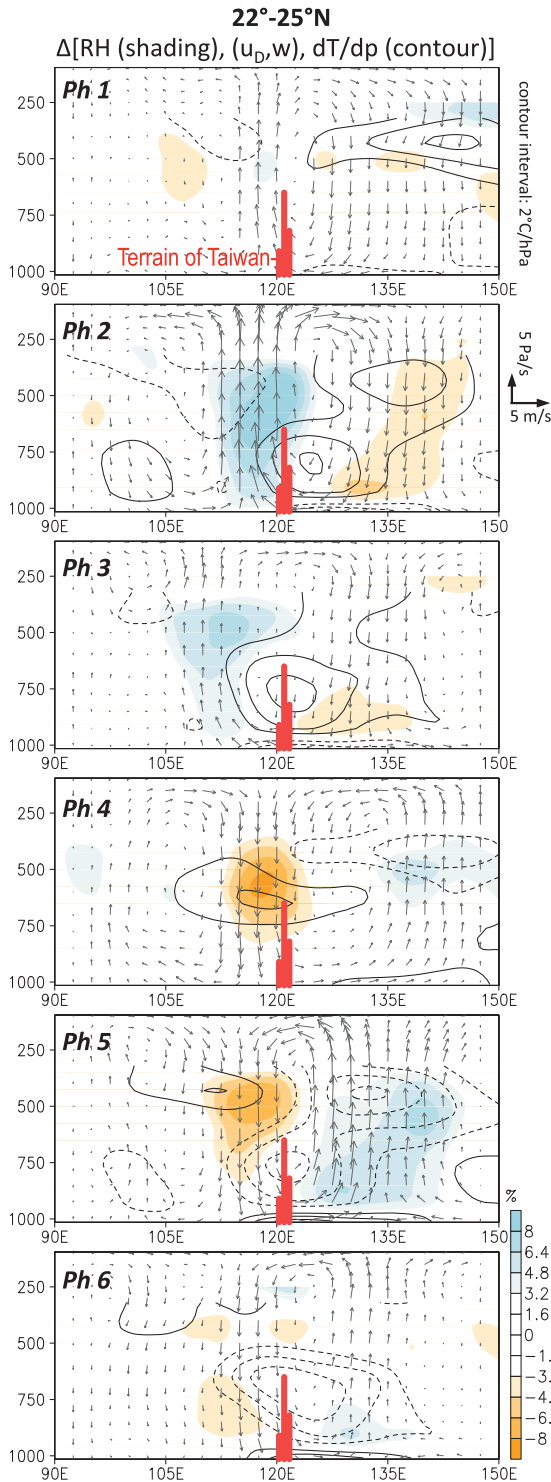
FIG. 4. (a) Illustration of the six evenly divided phases within the biweekly mode. (b) Composite 850-mb streamfunction anomalies at each phase with a contour interval of $2 \times 10^6 \, \text{m}^2 \, \text{s}^{-1}$. (c) Composite PDA over Taiwan during each phase. (d) Composite hourly precipitation evolution over Taiwan during each phase.

22°-25°N

Δ[RH (shading), (u_D,w), dT/dp (contour)]

FIG. 5. Composite anomalies of relative humidity (shading), *dT/dp* (contour, zero omitted), and the zonal divergent circulation vectors averaged across 22°–25°N for the six phases of the biweekly mode. Red bars near 120°E indicate the terrain in Taiwan.

humidity, divergent circulation (i.e., zonal divergent wind and vertical velocity), and temperature lapse rates averaged across Taiwan (i.e., from 22° to 25°N). These composite fields were not filtered; only the summer means were removed to display the anomalies. During phases 1–3, enhanced upward motion is present west of Taiwan and is coupled with increasing relative humidity and instability in the middle and lower troposphere. Phase 2 features favorable conditions for diurnal convection consisting of enhanced upward velocity and relatively moist, unstable air around Taiwan. These conditions are known to increase the diurnal convection activity in northern Taiwan (Lin et al. 2012). In contrast, phase 5 exhibits an unfavorable environment for diurnal convection due to enhanced subsidence, as well as drier and more stable air. These favorable and unfavorable conditions for diurnal convection alternate and are associated with the westward propagation of the QBW mode.

For validation purposes, the association between the diurnal convection activity and the QBW mode was examined by further using the daily index of PDA. First, we computed the area-averaged PDA (as in Fig. 4c) for each day; second, we constructed the composite of the filtered 850-mb streamfunction based upon the daily PDA evolution using the peak PDA as day 0 with a 3-day average. The dates of active synoptic weather were removed from this composite. Such an analysis led to a PDA-based composite and was used as a comparative against the composite based on *v* wind (Fig. 4b). As is shown in Fig. 6, the evolution of the bandpass-filtered streamfunction anomalies from day −3 through day +3 coincides well with the phase 1–3 circulation patterns given in Fig. 4b. Focusing on the 10–20-day oscillation, Jiang and Lau (2008) found that a circulation evolution similar to that described in Fig. 6 could excite a trans-Pacific wave train toward western North America. Moreover, of note, are the enhanced westerly and southwesterly flows over the Indochina Peninsula and the South China Sea at days −3 and 0, suggesting a coupling of the QBW mode with the monsoonal southwesterlies. Such a coupling enhances the midtropospheric moisture necessary for the development of diurnal convection. The associated moistening in the lower troposphere concurs within phase 2, as is revealed in Fig. 5.

c. Empirical relationship

The marked correspondence between the QBW mode and the diurnal convection activity suggests the possibility of building an empirical relationship. Given the prominent dipole structure of the circulation anomalies, as was evident in Figs. 3b (day 0), 4b (phases 2 and 5),

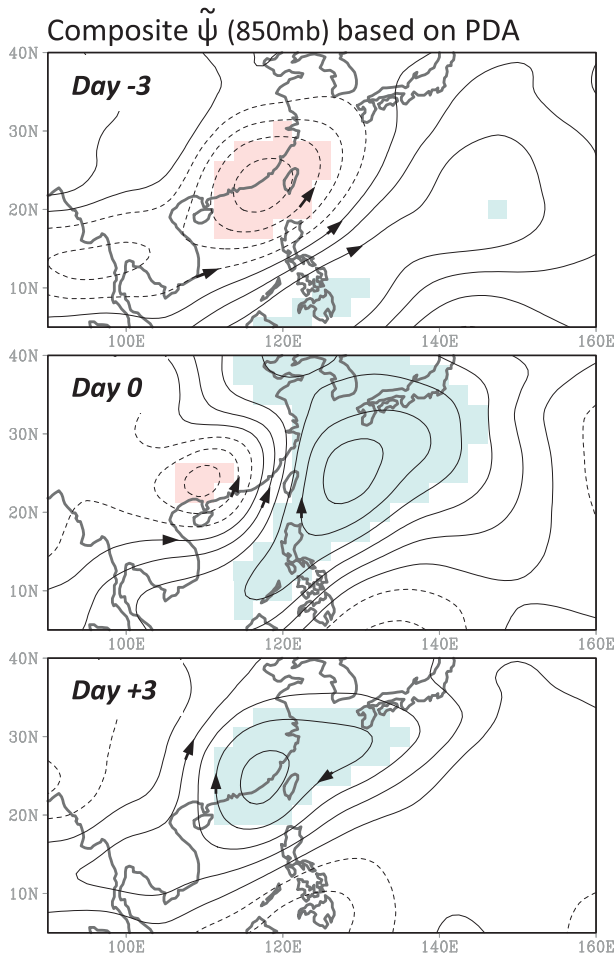## Composite $\tilde{\psi}$ (850mb) based on PDA

FIG. 6. Composite 850-mb streamfunction anomalies ($\tilde{\psi}$) based on the PDA index with 3-day lags (shown at top left). The values that are significant at the 95% level are color shaded.
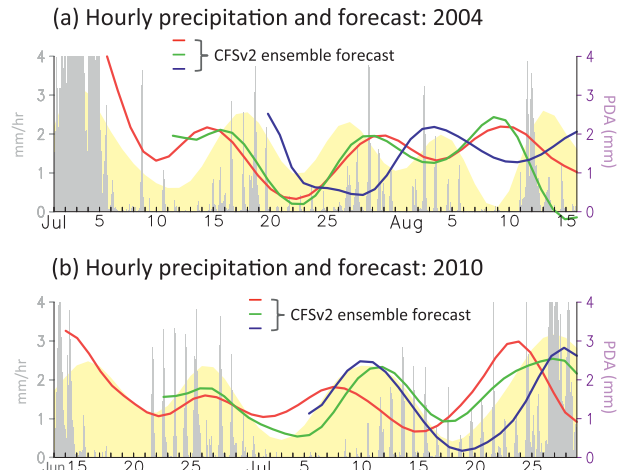

FIG. 7. As in Fig. 2, but with hourly precipitation plotted as a gray histogram, overlaid with the PDA estimated by CFSR (yellow shading), and predictions by three CFSv2 ensemble forecasts (color lines) initialized on the day where the lines began.

The PDA^E (i.e., estimated PDA) is presented as a shaded curve in Fig. 7 and overlaid on hourly precipitation for two instances: years 2004 and 2010. In 2004, the three diurnal convection episodes were essentially captured by the PDA^E. During the middle episode (25–31 July), the PDA^E was offset by 3 days. In 2010, the PDA^E appears to have underestimated the first episode (22–30 June) and was offset by a half phase during the second episode (10–18 July). In the long term, however, the occurrence of diurnal convection episodes tends to be in phase with the PDA^E; this is evident in the PDA composite in Fig. 6. However, as can be seen in Fig. 7, the PDA^E also covers the tropical cyclone/depression (TC/TD) events, which may suggest modulation of the tropical activity over the northwestern Pacific by the QBW mode (e.g., Ko and Hsu 2006). Thus, this circulation-based index might also be applicable for tropical cyclone forecasting.

4. CFSv2 forecast evaluation

Following the PDA^E application as was shown in Fig. 7, we next evaluated the CFSv2 reforecasts of $\Delta\tilde{\psi}$ using Eq. (1). Here, we used a 5-day ensemble of the CFSv2 forecast ending on the fifth day; this ensemble approach was composed of 20 members from the 6-hourly outputs for 5 days. The adoption of this 5-day ensemble was empirical (results not shown), and it was found that the effect of the ensemble size on forecast skill becomes insignificant after 16 (i.e., 4 days). In fact, when the ensemble size reaches 24 (i.e., 6 days), the

and 6 (day 0), we derived the filtered 850-mb streamfunction differences between the central locations of the circulation dipole—one centered at 22.5°N and 130°E (east of Taiwan) and the other centered at 22.5°N and 110°E (west of Taiwan) using a 5°-box average; this differential streamfunction is denoted as $\Delta\tilde{\psi}$. The use of the streamfunction difference here not only delineates the circulation pattern that is indicative of the meridional wind anomalies but it also connects to the monsoon trough variation. Based upon the daily values of $\Delta\tilde{\psi}$ and PDA, we derived a second-order polynomial regression fit to estimate the PDA:

$$\text{PDA}^E = 0.16\Delta\tilde{\psi}^2 + 0.96\Delta\tilde{\psi} + 1.14, \qquad (1)$$

where $\Delta\tilde{\psi}$ is scaled down by a factor of 10^{-6}. The regression model of Eq. (1) had a greater R^2 value (0.88) when compared to that of a purely linear model (0.62).

forecast skill begins to drop, probably due to earlier forecasts decreasing the skill. As an example, three random CFSv2 forecasts of the PDA are shown in Fig. 7a for the summer of 2004. The forecast initialized on 2 July (red line, representing the ensemble of 28 June–2 July) captures the 15–20 July episode as well as the 26–30 July episode. A forecast initialized on 11 July (green line) is in agreement with that initialized on 2 July. However, a forecast initialized on 20 July (blue line) fails to predict the 26–30 July episode, yet it captures the following episode on 1–5 August. For 2010 (Fig. 7b), three random CFSv2 forecasts reveal a more stable performance by capturing the diurnal convection episodes 20–30 days after. However, both the PDA estimate and CFSv2 forecasts tend to underestimate (or smooth out) the amplitude of individual events; this drawback has to be compensated for by daily weather forecasts for the next 3–5 days. Noteworthy in 2010 is the forecast initialized on 5 July (blue line), which not only captures the diurnal convection episode in July but also coincides with the TC/TD event in late July.

To quantitatively evaluate the forecast skill, we examined the predicted PDA^E for the summers of 1999–2010 against (a) the observed PDA^E, (b) individual events of diurnal convection, and (c) episodes of sequential events. For the first case, on the day when both the observed and predicted PDA^Es were greater than 1 mm, or both were less than 1 mm, the day was defined as a "hit"; otherwise, the day was a "miss." In the second case, individual diurnal convection events were defined as the island-wide average rainfall in the noon-to-midnight hours was twice as great as that during the morning hours (0500–1100 LT) while the morning rainfall accumulation was less than 1 mm. Additionally, on a diurnal convection event when the predicted PDA^E was greater than 1 mm, or on a dry day (daily rainfall < 1 mm) when the predicted PDA^E was less than 1 mm, then the event was defined as a hit; otherwise, the event was a miss. For the final case, an episode was defined as being composed of diurnal convection events occurring consecutively for four or more days. Moreover, on either the second or the third day of the episode, if the predicted PDA^E was greater than 1 mm, then this event was defined as a hit and, otherwise, a miss. For any diurnal convection event lasting longer than 4 days, the hits and misses were computed independently within each 4-day segment.

After obtaining hits and misses, we constructed a simple score,
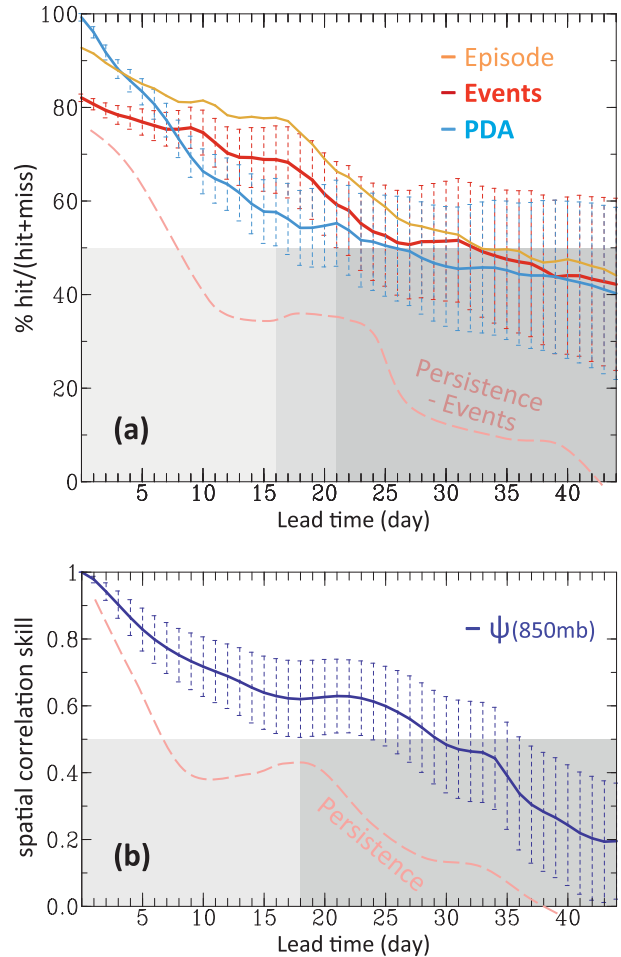
$$score = \frac{hit}{(hit + miss)}\%, \quad (2)$$

FIG. 8. (a) Score of CFSv2 forecast vs lead time in days represented by the percentage of hit/(hit+miss) based on the PDA (cyan), individual diurnal convection events (red), episodes of events lasting 4 days or longer (orange), and persistence forecasts for individual events (pink). Error bars indicate one standard deviation. Gray areas indicate the effective forecast skill. (b) Spatial correlation skill of 850-mb ψ from CFSv2 (blue) and persistence (pink) forecasts at different lead times.

to evaluate the CFSv2 forecast skill of diurnal convection via Eq. (1). Here, active weather events were excluded. Figure 8a shows the score of the CFSv2 prediction with respect to lead time in days. For the PDA^E versus PDA^E prediction (cyan line; Fig. 8a), the mean score decreases quickly toward day 10 but remains above 50% until about day 25. If we define the effective lead time as the duration in which the error bar of the forecast score is greater than 50%, then there is an effective 16-day lead time associated with this PDA prediction. For the prediction of individual diurnal convection "events" (red line), the score surpasses the PDA score after day 7 and exhibits a 21-day effective lead time. For the prediction of diurnal convection episodes (orange

line), the score is similar to, but consistently higher than, the prediction of events with a 24-day effective lead time (error bars not shown). In comparison, the score of persistence prediction for the events category (dashed line) decreases quickly below 50% by day 8 and exhibits an oscillatory pattern with a frequency of about 20 days. Such an oscillatory pattern is possibly a reflection of the ISO signal embedded within the diurnal convection activity (cf. Fig. 2).

The forecast scores in Fig. 8a are directly related to the forecast skill in the 850-mb circulation anomalies, or $\Delta\tilde{\psi}$. Thus, we examined the spatial correlation skill of the 850-mb streamfunction $\psi (=\tilde{\psi} + \overline{\psi}$, where $\overline{\psi}$ is the seasonal mean); this is shown in Fig. 8b. We focused on the domain 5°–35°N, 100°–150°E that approximates the dimension of the QBW mode dipole as was the case in Fig. 3b. The correlation skill was computed for the entire summer (92 days). The correlation skill in Fig. 8b reveals a similar effective lead time of about 18 days, based on the duration in which the error bar remains above 0.5. In contrast, the skill of persistence forecast of ψ (i.e., predicting the same ψ pattern for the next day) declines much more quickly than that of the CFSv2 forecast and reveals an oscillatory feature as well.

To substantiate the forecast of the QBW mode's propagation feature, Fig. 9 presents the longitude–time diagram of observed $\tilde{\psi}$ (shading) averaged across 20°–25°N for 2004 (panel a) and 2010 (panel b); we also display $\tilde{\psi}$ in 2008 (panel c), during which a tropical cyclone took place. Three CFSv2 forecasts of $\tilde{\psi}$ are overlaid with a 6-day interval on initial time (contour). Corresponding to the QBW mode (Fig. 3), Fig. 9a shows a westward propagation of $\tilde{\psi}$ through Taiwan (~120°E). The CFSv2 produces consistent phases in the propagation and alternation of positive–negative $\tilde{\psi}$ anomalies out to 2–3 weeks; this is supportive of the correlation skill shown in Fig. 8b. In 2010 when the QBW mode was weak (Fig. 9b), the CFSv2 performance is not as good as was the case in 2004. However, in 2008 when the QBW mode was strong while Typhoon Fung-Wong was embedded in one of the cyclonic cells (Fig. 9c), the CFSv2 exhibits a relatively good level of skill out to 3 weeks. The results are therefore suggestive of the correspondence between the CFSv2 forecast skill and the QBW mode's amplitude or activity.

5. Summary and conclusions

The occurrence of diurnal/afternoon convection in Taiwan undergoes substantial modulation from the tropical intraseasonal oscillation. Specifically, the QBW

mode that is active in summer over the western North Pacific plays a significant role in the formation of episodic diurnal convection. When the cyclonic circulation of the QBW mode is located west of Taiwan and is followed by an anticyclonic circulation to the east, the diurnal convection activity tends to intensify and persist for as long as this circulation dipole is in place, which is about 4–7 days. Synoptically, this situation reflects the enhanced subtropical anticyclone (leading to fair-weather conditions) and increased monsoon southwesterly winds (i.e., moistening of the lower troposphere) that are conducive to diurnal convection over Taiwan. The opposite situation, that of an anticyclonic cell to the west and a cyclonic cell to the east of Taiwan, suppresses the diurnal convection activity for a sustained period of time. These features suggest that the QBW can affect weather in Taiwan even without initiating storms or tropical cyclones.

Because forecasting the episodic feature of diurnal convection, which occurs within the QBW time frame, is beyond the Lorenz limit in weather forecasting, a climate prediction approach was tested in this study. Using the CFSv2 to derive the precipitation diurnal amplitude (PDA) from low-level circulation fields, through the empirical relationship of Eq. (1), it was found that the CFSv2 forecast had an effective lead time of 16–24 days for the potential (timing and duration) of the diurnal convection episodes. Such forecast skill is closely related to the CFSv2's performance in forecasting the QBW mode in the western North Pacific. The results presented here therefore suggest that short-term climate prediction of diurnal convection episodes in Taiwan is feasible.

It is intended that the short-range climate forecast of diurnal convection, as documented here, will be integrated with existing weather forecast procedures. Currently, the CWB of Taiwan exercises a somewhat ambiguous operational procedure to forecast diurnal convection, consisting of 1) the position of the subtropical height located to the east of Taiwan as judged by the 5880-m contour at 500 mb, 2) increased moisture content at 850 mb in concert with prevailing southwesterly winds, and 3) the computation of convective available potential energy (CAPE) from the morning sounding in Taipei [World Meteorological Agency (WMO) ID 46692] to be greater than $1000 \, J \, kg^{-1}$. Future work should involve combining recently developed objective schemes, such as that documented in Lin et al. (2012), to construct operational long- and/or short-term forecasts for diurnal convection.
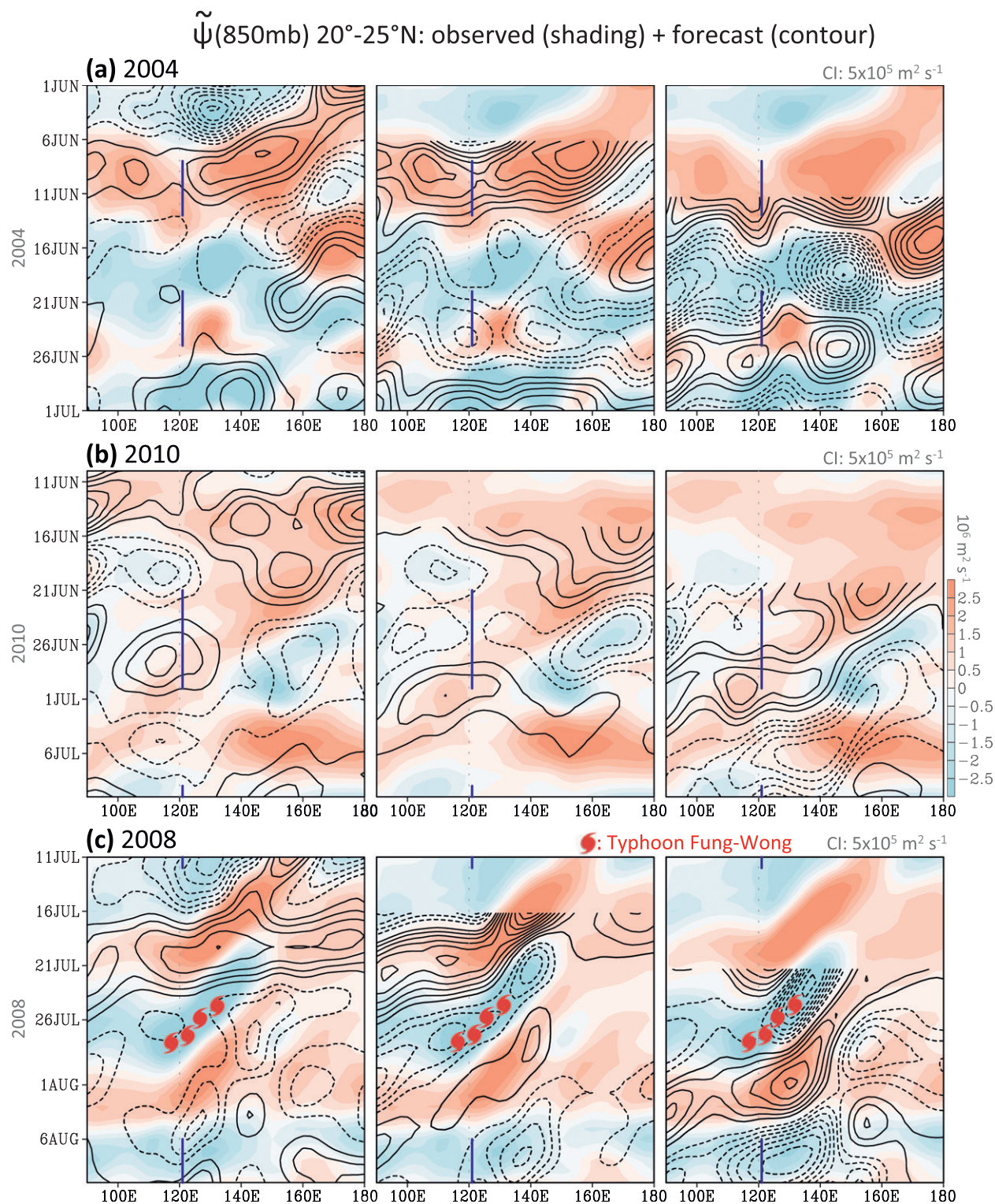
$\widetilde{\psi}$(850mb) 20°-25°N: observed (shading) + forecast (contour)

FIG. 9. Longitude–time diagrams of 850-mb ψ averaged across 20°–25°N from CFSR (shading) and CFSv2 (contour) ensemble forecasts at three initial times from left to right with a 6-day interval, for (a) 2004, (b) 2010, and (c) 2008. Blue lines along 120°E indicate diurnal convection episodes. The typhoon symbol in (c) indicates Typhoon 9, which passed over Taiwan during late July 2008.

REFERENCES

Agudelo, P. A., J. A. Curry, C. D. Hoyos, and P. J. Webster, 2006: Transition between suppressed and active phases of intraseasonal oscillations in the Indo-Pacific warm pool. *J. Climate,* **19,** 5519–5530.

Chang, C.-P., Ed., 2004: *East Asian Monsoon.* World Scientific Series on Asia-Pacific Weather and Climate, Vol. 2, World Scientific Publishing, 572 pp.

Chen, T.-C., M.-C. Yen, J.-C. Hsieh, and R. W. Arritt, 1999: Diurnal and seasonal variations of the rainfall measured by the automatic rainfall and meteorological telemetry system in Taiwan. *Bull. Amer. Meteor. Soc.,* **80,** 2299–2312.

——, ——, and S.-P. Weng, 2000: Interaction between the summer monsoons in East Asia and the South China Sea: Intraseasonal monsoon modes. *J. Atmos. Sci.,* **57,** 1373–1392.

——, S.-Y. Wang, W.-R. Huang, and M.-C. Yen, 2004a: Variation of the East Asian summer monsoon rainfall. *J. Climate,* **17,** 744–762.

——, ——, M.-C. Yen, and W. A. Gallus, 2004b: Role of the monsoon gyre in the interannual variation of tropical cyclone formation over the western North Pacific. *Wea. Forecasting,* **19,** 776–785.

Cressman, G. P., 1959: An operational analysis system. *Mon. Wea. Rev.,* **87,** 367–374.

Ding, Y., and J. C.-L. Chan, 2005: The East Asian summer monsoon: An overview. *Meteor. Atmos. Phys.,* **89,** 117–142.

Fukutomi, Y., and T. Yasunari, 1999: 10–25 day intraseasonal variations of convection and circulation over East Asia and western North Pacific during early summer. *J. Meteor. Soc. Japan,* **77,** 753–769.

Hendon, H. H., B. Liebmann, M. Newmann, J. D. Glick, and J. E. Schemm, 2000: Medium-range forecast errors associated with active episodes of the Madden–Julian oscillation. *Mon. Wea. Rev.,* **128,** 69–86.

Hsu, H.-H., 2005: East Asian monsoon. *Intraseasonal Variability in the Atmosphere–Ocean Climate System,* W. K. M. Lau and D. E. Waliser, Eds., Springer, 389–424.

——, and C.-H. Weng, 2001: Northwestward propagation of the intraseasonal oscillation in the western North Pacific during the boreal summer: Structure and mechanism. *J. Climate,* **14,** 3834–3850.

Huang, W.-R., and J. C.-L. Chan, 2011: Seasonal variation of diurnal and semidiurnal rainfall over southeast China. *Climate Dyn.,* **39,** 1913–1927, doi:10.1007/s00382-011-1236-5.

Ichikawa, H., and T. Yasunari, 2006: Time–space characteristics of diurnal rainfall over Borneo and surrounding oceans as observed by TRMM-PR. *J. Climate,* **19,** 1238–1260.

——, and ——, 2008: Intraseasonal variability in diurnal rainfall over New Guinea and the surrounding oceans during austral summer. *J. Climate,* **21,** 2852–2868.

Jiang, X., and N.-C. Lau, 2008: Intraseasonal teleconnection between North American and western North Pacific monsoons with 20-day time scale. *J. Climate,* **21,** 2664–2679.

——, T. Li, and B. Wang, 2004: Structures and mechanisms of the northward propagating boreal summer intraseasonal oscillation. *J. Climate,* **17,** 1022–1039.

Johnson, R. H., and P. E. Ciesielski, 2002: Characteristics of the 1998 summer monsoon onset over the northern South China Sea. *J. Meteor. Soc. Japan,* **80,** 561–578.

Kim, D., and Coauthors, 2009: Application of MJO simulation diagnostics to climate models. *J. Climate,* **22,** 6413–6436.

Ko, K. C., and H. H. Hsu, 2006: Sub-monthly circulation features associated with tropical cyclone tracks over the East Asian monsoon area during July–August season. *J. Meteor. Soc. Japan,* **84,** 871–889.

Lau, K.-M., and P. H. Chan, 1986: Aspects of the 40–50 day oscillation during the northern summer as inferred from outgoing longwave radiation. *Mon. Wea. Rev.,* **114,** 1354–1367.

——, and D. E. Waliser, Eds., 2005: *Intraseasonal Variability in the Atmosphere–Ocean Climate System.* Springer, 425 pp.

——, and Coauthors, 2000: A report of the field operations and early results of the South China Sea Monsoon Experiment (SCSMEX). *Bull. Amer. Meteor. Soc.,* **81,** 1261–1270.

Li, J., Y.-L. Chen, and W.-C. Lee, 1997: Analysis of a heavy rainfall event during TAMEX. *Mon. Wea. Rev.,* **125,** 1060–1081.

Lin, J.-L., and Coauthors, 2006: Tropical intraseasonal variability in 14 IPCC AR4 climate models. Part I: Convective signals. *J. Climate,* **19,** 2665–2690.

Lin, P.-F., P.-L. Chang, B. J.-D. Jou, J. W. Wilson, and R. D. Roberts, 2011: Warm season afternoon thunderstorm characteristics under weak synoptic-scale forcing over Taiwan Island. *Wea. Forecasting,* **26,** 44–60.

——, ——, ——, ——, and ——, 2012: Objective prediction of warm season afternoon thunderstorms in northern Taiwan using a fuzzy logic approach. *Wea. Forecasting,* **27,** 1178–1197.

Lin, S.-C., and M.-T. Kueh, 2003: A modeling diagnosis of the development of mesoscale convective systems over the South China Sea during the summer monsoon onset in 1998. *Terr. Atmos. Oceanic Sci.,* **14,** 369–399.

Matsumoto, J., 1989: Heavy rainfalls over East Asia. *Int. J. Climatol.,* **9,** 407–423.

Nitta, T., 1987: Convective activities in the tropical western Pacific and their impact on the Northern Hemisphere summer circulation. *J. Meteor. Soc. Japan,* **65,** 373–390.

Saha, S., and Coauthors, 2006: The NCEP Climate Forecast System. *J. Climate,* **19,** 3483–3517.

——, and Coauthors, 2010: The NCEP Climate Forecast System Reanalysis. *Bull. Amer. Meteor. Soc.,* **91,** 1015–1057.

Slingo, J. M., and Coauthors, 1996: Intraseasonal oscillations in 15 atmospheric general circulation models: Results from an AMIP diagnostic subproject. *Climate Dyn.,* **12,** 325–357.

Straub, K. H., and G. N. Kiladis, 2003: The observed structure of convectively coupled Kelvin waves: Comparison with simple models of coupled wave instability. *J. Atmos. Sci.,* **60,** 1655–1668.

Vitart, F., 2009: Impact of the Madden–Julian Oscillation on tropical storms and risk of landfall in the ECMWF forecast system. *Geophys. Res. Lett.,* **36,** L15802, doi:10.1029/2009GL039089.

Waliser, D. E., 2012: Predictability and forecasting. *Intraseasonal Variability in the Atmosphere–Ocean Climate System,* K.-M. Lau and D. E. Waliser, Eds., Springer, 433–468.

——, W. Stern, S. Schubert, and K. M. Lau, 2003: Dynamic predictability of intraseasonal variability associated with the Asian summer monsoon. *Quart. J. Roy. Meteor. Soc.,* **129,** 2897–2925.

Wang, B., and X. Xie, 1997: A model for the boreal summer intraseasonal oscillation. *J. Atmos. Sci.,* **54,** 72–86.

——, and LinHo, 2002: Rainy season of the Asian–Pacific summer monsoon. *J. Climate,* **15,** 386–398.

Wang, C.-C., and W.-M. Huang, 2009: High-resolution simulation of a nocturnal narrow convective line off the southeastern coast of Taiwan in the mei-yu season. *Geophys. Res. Lett.,* **36,** L06815, doi:10.1029/2008GL037147.

Wang, S.-Y., and T.-C. Chen, 2008: Measuring East Asian summer monsoon rainfall contributions by different weather systems over Taiwan. *J. Appl. Meteor. Climatol.,* **47,** 2068–2080.

Weaver, S. J., W. Wang, M. Chen, and A. Kumar, 2011: Representation of MJO variability in the NCEP Climate Forecast System. *J. Climate,* **24,** 4676–4694.

Yeh, H.-C., and Y.-L. Chen, 1998: Characteristics of rainfall distributions over Taiwan during the Taiwan Area Mesoscale Experiment (TAMEX). *J. Appl. Meteor.,* **37,** 1457–1469.

Zhang, Q., and H. Van den Dool, 2012: Relative merit of model improvement versus availability of retrospective forecasts: The case of Climate Forecast System MJO prediction. *Wea. Forecasting,* **27,** 1045–1051.